CHEMICAL ENGINEERING COMMUNICATIONS
https://doi.org/10.1080/00986445.2025.2549909

Simulation study on pressure distribution and pressure drop in corrugated plate packing with different structural parameters

Enhua Zheng[a], Lina Tang[b], Zhixiang Xia[a], Mengxiang Fang[a], Ximing Hu[a], Yutao Xia[a], and Tao Wang[a]

[a]State Key Laboratory of Clean Energy Utilisation, Zhejiang University, Hangzhou, China; [b]Zhejiang Zheneng Technology and Environment Group Co., Ltd., Hangzhou, China

ABSTRACT

Structured packing is extensively employed in gas-liquid separation processes due to its provision of a large specific surface area and elevated porosity. However, this configuration concurrently induces an increase in system pressure drop. A comprehensive understanding of the influence of packing structural parameters on hydrodynamic characteristics becomes imperative for achieving enhanced separation efficiency and optimized energy consumption in industrial applications. This study constructed a high-fidelity corrugated double plate model considering parameters such as holes and plate thickness. A systematic numerical investigation employing the k-ω shear stress transport model was conducted to comprehensively evaluate the hydrodynamic effects of key geometric parameters (thickness, hole diameter, hole spacing, corrugated inclination angle, and corrugated tooth angle) on the double-plate model of corrugated plate packing. The reliability of the model was confirmed through comparing it with previous studies. Qualitative and quantitative analyses of the internal flow field and pressure distribution were conducted under different geometric and structural parameters of the double-plate model. The underlying mechanisms of different structural parameters on the dry pressure drop in a corrugated plate were determined. The influence of each parameter on packing performance was explored. A predictive method for dry pressure drop was proposed. These results hold crucial implications for elucidating the influence mechanisms of structural parameters on packing performance and for optimizing and designing new packings to reduce energy consumption.

KEYWORDS

CFD simulation; structured packing; pressure distribution; pressure drop; corrugated plate

Introduction

Structured packing columns are commonly used in gas-liquid separation processes, where the structured packing provides an extensive mass transfer area and high porosity to facilitate gas-liquid phase interactions. Structured packing typically consists of corrugated sheets, grids, or other geometrically ordered arrangements with specific wave patterns or ridges, achieving high specific surface area and porosity through periodic organization. Currently, various structured packings including the high-capacity and high-performance Montz-pak and Mellapak series (Amini et al. 2016), have been implemented on a large scale across critical separation domains such as distillation, absorption, extraction, and carbon capture operations (Sebastia-Saez et al. 2015). However, the complex geometry of structured packings means their hydrodynamic characteristics still require more comprehensive investigation.

Over the last two decades, extensive experimental and numerical investigations have been dedicated to optimize the packing performance. Notably, experiment combined with empirically derived correlations have emerged as indispensable methodologies for predicting the hydrodynamic performance of packing (Billet 1987; Fair et al. 2000; Roselló Segado et al. 2002; Tsai et al. 2011). Fair et al. investigated the pressure loss, capacity, and mass transfer efficiency by changing pressure, corrugation angle, surface area, and surface design, which were employed to forecast the hydraulic and mass transfer performances (Fair et al. 2000). Zakeri et al. studied the pressure drop in three different commercially packings, and the results showed that both dry and wet pressure drops were functions of the gas and liquid flow rates (Zakeri

CONTACT Mengxiang Fang mxfang@zju.edu.cn Institute for Thermal Power Engineering, Zhejiang University, Hangzhou 310027, China.

et al. 2012). Olujić et al. introduced the Delft model by investigating the influence of the corrugation angle and additional geometric structures on the hydrodynamic and mass transfer properties of packing, and they adjusted the geometric shapes to achieve an increase in capacity (Olujić et al. 2000; Olujic et al. 2001). Studying the hydrodynamic performance of corrugated plates requires a systematic study of corrugated plate parameters, but experimental validation alone is insufficient (Haroun and Raynal 2016).

Recently, the computational fluid dynamics (CFD) method has become a powerful tool and is widely used to study the hydrodynamic characteristics inside structural packing. The CFD enables structured packing analysis across scales [small-scale (Larachi et al. 2003; Macfarlan et al. 2021, 2022; Said et al. 2011), mesoscale (Olenberg and Kenig 2020; Raynal and Royon-Lebeaud 2007), and large-scale (Amini et al. 2016; Isoz and Haidl 2018; Olujić et al. 2015; Sun et al. 2021a; Wang et al. 2022)], overcoming experimental limitations. Petre et al. and Larachi et al. were the first to conduct numerical research on dry pressure drop, they proposed that structured packings can be divided into four distinct fundamental units corresponding to four primary packing lregions. This helped to reduce the computational burden, in contrast to simulating the entire column. The total dry pressure drop was calculated using the algebraic summation of the dry pressure drops across the four regions (Larachi et al. 2003; Petre et al. 2003). Amini et al. employed a CFD model to conduct an experimental performance assessment of a novel structured packing; however, the CFD estimates of the packing's dry pressure loss differed from the experimental data by up to 50% (Amini et al. 2016). Fard et al. simulated the pressure drop and mass-transfer efficiency through a packing column. The average relative error between the experimental and the predicted dry pressure drop data was determined to be 20.3% (Haghshenas Fard et al. 2007). Structured packing often involved two-phase flow (gas and liquid) in real applications, and single-phase simulation was acknowledged as a foundation of two-phase flow. There are certain deviations in the previous research results. The reason is that the research objects were mainly focused on the fluid channel unit between the two corrugated plates or the packing block structure. However, the fluid channel unit ignored plate thickness and openings, the packing block structure was just repetitions of unit structures. This study employed a double-plate flow unit model to investigate the dry pressure drop of packings. The model replicated the true structure of corrugated plates (including holes and plate thickness), which reduced the relative error of the data.

To investigate the influence of structural parameters on the hydrodynamic performance of packing, extensive research has been conducted by numerous scholars. Isoz and Haidl investigated the dry pressure drop across structured packing with different hole inclination, hole density, and packing surface area. They concluded that in terms of dry pressure loss, the channel inclination and the geometric area density of the packing are more influential than the packing perforation. However, the dry pressure loss of highly perforated packings is significantly lower than that of non-perforated packings (Isoz and Haidl 2018). Sun et al. analyzed how thickness, inclination, and perforations impact hydrodynamics. While perforations increase porosity, they also raise pressure drop by ∼10% (Sun et al. 2021a). Olujić et al. examined the effects of packing surface characteristics such as hole configuration and corrugation angle through a combination of experimental and modeling approaches. They determined that for enhanced gas-liquid contact, an optimal corrugation angle of 45° was preferred for corrugated plates (Olujić et al. 2015). Wang et al. examined the effects of the wavelength, amplitude, angle, and position on the dry pressure drop within a packing column using the CFD method. An increase in the wavelength, amplitude, and ripple angle led to a decrease in the pressure drop (Wang et al. 2022). Macfarlan et al. studied the geometric aspects of structured packing by systematically varying the channel opening angle, specific packing area, and channel inclination angle, in order to identify the geometry that optimizes mass transfer efficiency while minimizing pressure drop (Macfarlan et al. 2021; 2022). Owens et al. fitted the relationship between gas phase loading and dry pressure drop to obtain the equation under the corresponding conditions, but did not consider the influence of structural parameters

(Owens et al. 2013). The aforementioned studies introduced the influence of structural parameters on packing pressure drop, yet most research effort predominantly focused on the overall pressure drop of packing (packing column), while lacking intuitive representation of pressure distribution within corrugated plates. Furthermore, the underlying mechanisms governing pressure drop variations in corrugated plates under diverse geometric parameters remain inadequately elucidated, accompanied by insufficient systematic theoretical analysis. Significantly, the quantitative correlation between packing pressure drop and structural parameters has not been comprehensively established with integrated consideration of multiple geometric factors.

In this study, based on the widely used Mellapak 250Y, the k-ω shear stress transport (SST) model was used to numerically study the high-fidelity double-plate model of corrugated packing by changing the structural parameters. The accuracy of the CFD model was verified by comparison with previous studies. By studying the internal flow field and pressure drop under different gas-phase loading factors in the double-plate model, the internal pressure distribution was visually displayed. Through qualitative and quantitative analyses, the influence of different geometric structure parameters (thickness, hole diameter and spacing, corrugated inclination, and tooth angle) on the pressure drop of the corrugated plate was obtained, and the influence mechanism of each parameter on packing performance was discussed. The numerical relationship between the pressure drop of the packing and the structural parameters was summarized, and the pressure drop prediction model was proposed. The aforementioned research is critically significant for both elucidating the influence mechanisms of structural parameters on the performance of corrugated packing and optimizing the design of structured packing.

Physical model and numerical method

Definition of the model geometry

To better reflect the flow characteristics of the fluid between the corrugated plates, the corrugated plate model established in this study restores the real structure of the corrugated plate, such as the holes and thickness (ignoring surface bumps and pits). Figure 1 shows the corrugated plate model and the schematic diagram of the structural parameters. The two adjacent corrugated plates are usually arranged in the form of staggered occlusion along the corrugated direction. In the corrugated plate, the wavelength B is the distance between the adjacent peaks of the corrugated plate, the peak height h is the height between the peak and the trough of the corrugated plate, S is the length of the corrugated hypotenuse, and the tooth angle β is the angle between the adjacent inclined edges of the corrugated plate. The tooth angle of the corrugated plate is related to the length of its inclined edge of the corrugated plate and the height of the wave peak. The actual measured initial structural parameters of the corrugated plate are: 14.8 mm corrugated bevel length S, 21.5 mm wavelength B, and 10.2 mm wave height h. Table 1 lists the value range of each parameter.

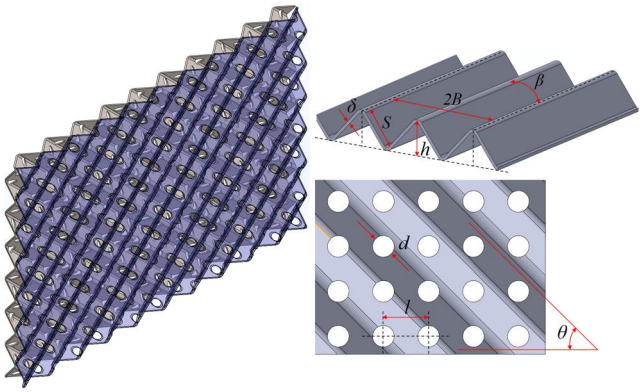

Figure 1. The geometric structural parameters of the corrugated plate packing.

Table 1. Structural parameters of corrugated plate used in simulation.

Corrugated plate properties	Value
Thickness δ (mm)	0.15, 0.2, 0.4, 0.8, 1.0, 1.2, 1.4
Hole diameter d (mm)	4, 5, 6, 7, 8
Hole spacing l (mm)	8, 10, 12.5, 16, 20
Corrugated inclination angle θ (°)	30, 40, 45, 50, 60, 70
Corrugated tooth angle β (°)	120, 100, 90, 80, 70, 60, 50, 40, 30

Computational domain and meshing

The complete-structured packing block model is relatively complex and huge, and its composition is mainly a repeated flow channel structure; therefore, the workload for restoring the overall structure is large. The unit form of the double-plate combination can not only reserve the necessary structural characteristics and geometric parameters of the real fluid channel, but also significantly avoid the waste of computing resources to enhance the computational efficiency of the model. The physical model of the double plate comprises two reversely combined corrugated plates and an outer wall structure, as shown in Figure 2(a). The physical model was extracted from the fluid domain to obtain the computational domain through pre-processing software. The width of the corrugated plate model, W, was 300 mm, and the height, H, was 200 mm. Owing to the existence of a corrugated structure, a regular gap is formed between the two single plates to form an area where the fluid passes. The overall size of the fluid domain was 300 mm · 240 mm · 23.4 mm, and the inlet and outlet were positioned 20 mm away from the corrugated plate, which was used to mitigate the influence of the inlet and outlet on the fluid flow process and improve the accuracy of the simulation (Ambekar et al. 2024).

Figure 2(b) shows the computational domain obtained by removing the solid structure from the physical model by preprocessing software. Owing to the complex geometry and large number of small details of the model in this study, when a tetrahedral mesh is used to divide the model, the number of meshes is large, and the mesh quality is poor. Nevertheless, we have elected to utilize a mesh generation methodology that incorporates both hexahedral and polyhedral elements. The resulting meshes exhibit a low element count and high quality, with adaptive refinement applied to regions of geometric complexity. The small diagram in Figure 2(b) shows the actual mesh inside the model.

Governing equations

In this research, steady-state and single-phase simulation were performed to investigate the dry pressure drop in corrugated plate, which requires simultaneous solutions to the continuity equation, momentum equation, and turbulence model. For the fundamental fluid flow, the continuity equation is as follows:

Mass conservation equation:

$$\frac{\partial \rho}{\partial t} + \nabla \cdot (\rho \boldsymbol{u}) = 0 \tag{1}$$

Momentum equation:

$$\frac{\partial (\rho \boldsymbol{u})}{\partial t} + \nabla \cdot (\rho \boldsymbol{u}\boldsymbol{u}) = -\nabla \cdot p + \mu \nabla^2 \boldsymbol{u} + \rho g + \boldsymbol{F} \tag{2}$$

where p, $\boldsymbol{u}$, μ, and ρg respectively represent static pressure, flow velocity, dynamic viscosity, and gravitational body force. $\boldsymbol{F}$ is the volume force source term, but the simulation in this study

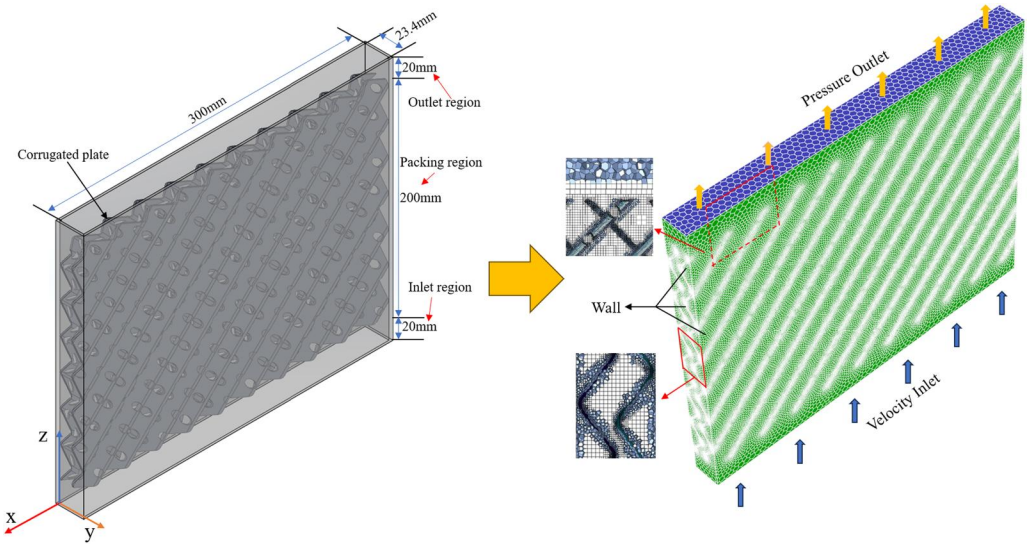

Figure 2. Computational domain and meshing. (a) Calculation model. (b) Mesh division and boundary condition.

involved a unidirectional flow of the gas phase; therefore, there is no need to add it. For steady-state simulations, the time-derivative term in Equations (1) and (2) was 0.

In the CFD model, the k-ω model includes the effects of low Reynolds number, compressibility, and shear flow, which is suitable for the calculation of mixed layer, wall-limited flow, and free shear flow. In contrast, the k-ω SST model incorporates a lateral dissipation derivative term and takes into account the transport equation for turbulent shear stress (Amini et al. 2016; Sun et al. 2021a, 2021b). The turbulence constants used were also different, and the scope of application was wider. Therefore, the k-ω SST model was selected with reference to the studies by Sun et al., Hosseini et al., Yang et al., and Said et al. The free flow in the boundary layer near the corrugated plate and channel formed by the packing corrugation can be properly modeled (Hosseini et al. 2012; Said et al. 2011; Sun et al. 2021a; Yang et al. 2024). The correlation of the k-ω SST model is expressed as:

$$\mu_t = \alpha^* \frac{\rho k}{\omega} \tag{3}$$

$$\frac{\partial(\rho\omega)}{\partial t} + \frac{\partial(\rho\omega u_i)}{\partial x_i} = \frac{\partial}{\partial x_i}\left(\Gamma_\omega \frac{\partial \omega}{\partial x_i}\right) + G_\omega - Y_\omega \tag{4}$$

$$\frac{\partial(\rho k)}{\partial t} + \frac{\partial(\rho k u_i)}{\partial x_i} = \frac{\partial}{\partial x_i}\left(\Gamma_k \frac{\partial k}{\partial x_i}\right) + G_k - Y_k + D_\omega \tag{5}$$

where μ_t is the turbulent viscosity, α^* is a coefficient, k refers to the kinetic energy, ω is the specific dissipation rate, Γ_ω and Γ_k are the effective diffusivities for ω and k, G_ω and G_k represent the generation of ω and k, Y_k and Y_ω account for the turbulent dissipation of k and ω, and D_k is the cross-diffusion.

Computational method

The calculation of the model requires setting the boundary conditions. The corrugated plate walls were defined as a nonslip wall boundary conditions. For gas phase inlet, the boundary condition was set to be velocity inlet, which was set to a constant volume fraction distribution and velocity. Whereas the outlet was defined as the pressure outlet with a gauge pressure (Figure 2b) (Singh et al. 2017; Yu et al. 2018). Simultaneously, the cross-sections were set at corresponding positions in the vertical and horizontal directions in the model unit to monitor and calculate the average pressure and pressure difference in the unit on the corresponding vertical and horizontal surfaces in the model. All simulations were performed utilizing ANSYS Fluent. The SIMPLE algorithm and second-order upwind difference format were used to solve pressure-velocity coupling. A pressure-based solver is used. To ensure the precision of convergence results, the selected convergence criterion is set to a residual value not exceeding 10^{-5}. Finally, initialization was performed from the gas inlet, and the model operation was started.

Results and discussion

In this section, we first introduce the results of mesh independence and model verification, which were achieved by which is done through comparing the pressure drop. Considering that the dry pressure drop is not only the most direct hydrodynamic performance index of the packing but also the basis of wet pressure drop to a certain extent, this study considers the dry pressure drop as the analysis object. The gas-phase load factor ($F_{factor} = u_G\sqrt{\rho_G}$) is used to measure the magnitude of gas flow rate. Here ρ_G represents the gas density, u_G is the gas velocity. The pressure drop is characterized as the ratio of the differential pressure to the packing height, where the pressure difference is between the inlet ($Z = 20$ mm) and outlet ($Z = 220$ mm) considering the effect of inlet on the pressure (Al-Maqaleh et al. 2022; Sebastia-Saez et al. 2015). The expression showed as Equation (6):

$$\Delta P/H = \frac{P_{\text{in}} - P_{\text{out}}}{H} \tag{6}$$

After the model validation, we introduce the effects of internal pressure distribution of corrugated plate and corrugated plate structural characteristics on pressure drop, and finally give a summary.

Mesh independence and model verification

The fineness of the mesh significantly influences the simulation process and results. Consequently,

a mesh independence verification study must be conducted to establish the critical mesh density threshold so as to achieve the optimal computational efficiency and accuracy. Figure 3 shows the pressure drop and relative deviation in the corrugated plate for different mesh numbers. At the beginning, the pressure drop increased with the mesh refinement. When the number of meshes is more than 2.5 million, the pressure drop did not vary significantly with an increase in the number of meshes, and the relative deviation of the pressure drop was less than 0.5% (Isoz and Haidl 2018). Therefore, this mesh parameter was used for mesh generation. The minimum size for the mesh elements had been set at 0.1 mm. As the structure parameters of corrugated plate were adjusted in this study, to preclude the confounding effects of differing mesh sizes arising from variations in model geometry on the fidelity of simulation results, consistent meshing parameters were used for subsequent mesh generation.

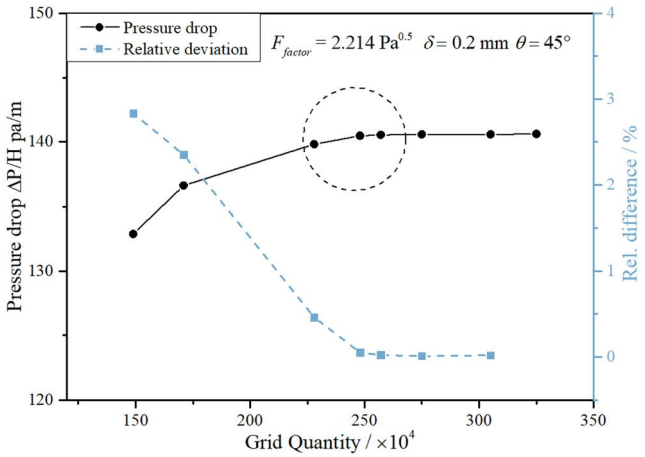

Figure 3. Mesh independence verification.

Figure 4(a) shows the sensitivity study of the computational domain dimensions (packing width, outlet region length, sheet number, and packing height) on pressure drop. We compared three working conditions with packing widths of 100 mm (100 mm × 240 mm × 23.4 mm), 200 mm (200 mm × 240 mm × 23.4 mm), and 300 mm (300 mm × 240 mm × 23.4 mm). The width was reduced from 300 mm to 200 mm, and the pressure drop increased by 18.4%. The width decreased from 200 mm to 100 mm, and the pressure drop increased by 24%. Considering the small deviation between the computational domain width of 300 mm and the results of Brunazzi et al. this width was adopted for subsequent simulations (Brunazzi and Paglianti 1997). Simulations of different outlet region lengths show that when the outlet length increases from 20 mm (300 mm × 240 mm × 23.4 mm) to 40 mm (300 mm × 260 mm × 23.4 mm), and then to 60 mm (300 mm × 280 mm × 23.4 mm), the average pressure drop decreases by 1.2% and 1%, respectively. The influence of the change in outlet length on the pressure drop characteristics can be ignored. Simulations were conducted on 2 pieces (300 mm × 240 mm × 23.4 mm), 3 pieces

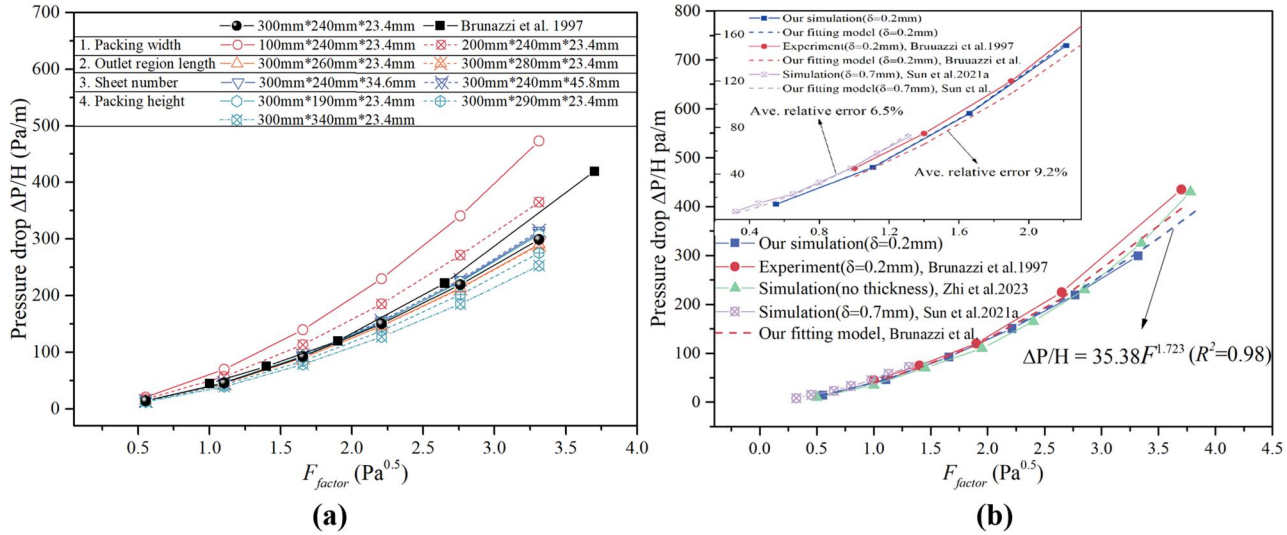

Figure 4. Model comparison verification. (a) Sensitivity analysis of model calculation domain size on results. (b) Comparison and verification between simulation results and literature results.

(300 mm × 240 mm × 34.6 mm), and 4 pieces (300 mm × 240 mm × 45.8 mm) of packing sheets, and the results showed a deviation of about 3% in pressure drop data for different numbers of pieces. Finally, four packing heights were investigated: 150 mm (300 mm × 190 mm × 23.4 mm), 200 mm (300 mm × 240 mm × 23.4 mm), 250 mm (300 mm × 290 mm × 23.4 mm), and 300 mm (300 mm × 340 mm × 23.4 mm). As height increased, the unit pressure drop progressively decreased: a 2.5% reduction occurred when height increased from 150 mm to 200 mm, followed by 7% reductions for each subsequent 50 mm increment. The commonly used packing height of 200 mm in engineering practice was selected for research.

To validate the accuracy of the model, a comparison was conducted between the simulated results of pressure drop as it relates to changes in the F_{factor} and the experimental data published by Brunazzi et al. as illustrated in Figure 4(b) (Brunazzi and Paglianti 1997). Brunazzi et al. used stainless steel 250Y. Our model in Figure 4(b) used the same plate thickness. As F_{factor} increases, our simulation values exhibit a very consistent trend with Brunazzi's experimental values, but the average pressure drop was approximately 12% lower. This is due to the increased pressure drop in the transition zone between adjacent packing layers. Additionally, a comparison was made with the simulation values reported by Sun et al. ($F_{factor}<1.4$, $\delta = 0.7$ mm). The average pressure drop was approximately 20% higher. This is attributed to the different thicknesses of corrugated plates. Compared with the simulation values reported by Zhi et al. the data deviation was smaller (Zhi et al. 2023). The four sets of data shown in the figure exhibit essentially the same trend, and our simulated values agree well with the experimental results of Brunazzi, which verifies the effectiveness of our model.

Internal pressure distribution of corrugated plate

Pressure distribution in different sections

This section presents qualitative and quantitative research on the pressure distribution at different cross-sectional positions. Qualitative analysis was mainly used to analyze the pressure distribution cloud diagrams of different sections, while the quantitative investigation involved detailed data analysis along the section's central axis in the specified direction.

Figure 5(a) shows the pressure distribution of the centerline of *YOZ* cross-section and Figure 5(b) shows the contour of the cross-section pressure distribution. To reduce the influence of the boundaries on both sides along the *X*-axis direction, cross-sections 10 mm from the boundary were taken for analysis. In the left figure, the *Z*-axis direction is divided into three regions: inlet,

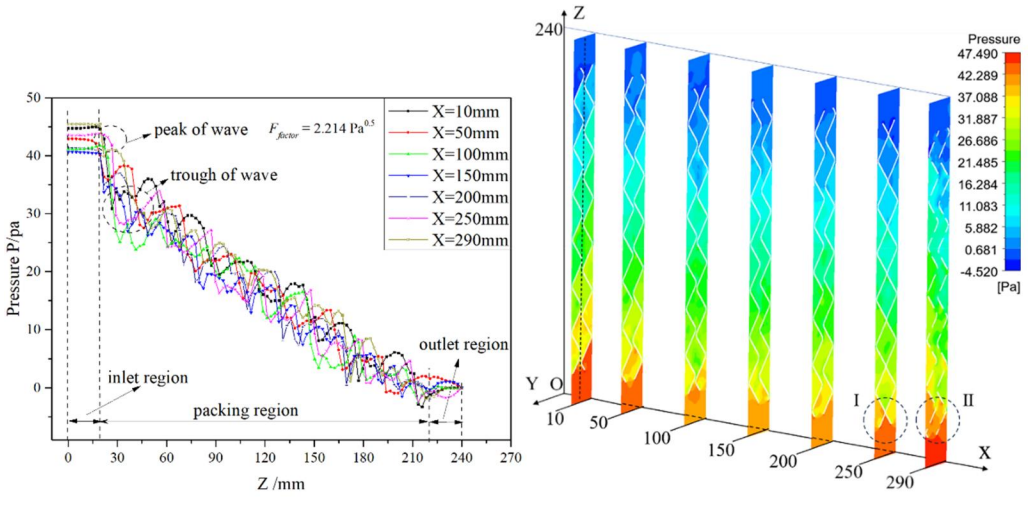

(a) (b)

Figure 5. Pressure distribution diagram of *YOZ* section at different locations. (a) Section centreline pressure distribution. (b) Contour of cross-sectional pressure distribution.

packing, and outlet. The pressure in the inlet region near the boundary on both sides was higher ($X = 10$ and 290 mm). The closer it is to the center, the smaller the pressure. The pressure changes at the centerline of the different sections in the packing area was wavy and gradually decreased. With an increase in Z, the overall trend decreased linearly (Sebastia-Saez et al. 2015). The lower pressure trough area is the area close to the corrugated plate wall (region I with $X = 250$ mm in Figure 5a and b). When the corrugated plate was further approached, the hindering pressure on the corrugated plate wall gradually increased but was much lower than the initial pressure (Figure 5b). The pressure drop was small and the pressure change near the hole was more uniform in the presence of corrugated plate holes (Region II shown in Figure 5a and b, $X = 290$ mm). Subsequently, the gas continued to touch the wall in the corrugated plate region and the pressure gradually decreased. There was no obvious pattern of pressure change near the outlet region, and there was a partial negative pressure area. Similar phenomena were observed in Liu et al.'s study (Liu et al. 2024). This is attributed to the acceleration or deceleration of the gas flow in the corrugated plate outlet area, and the rotation and counterflow of the gas in the negative pressure area, resulting in a local pressure reduction (Figure 6).

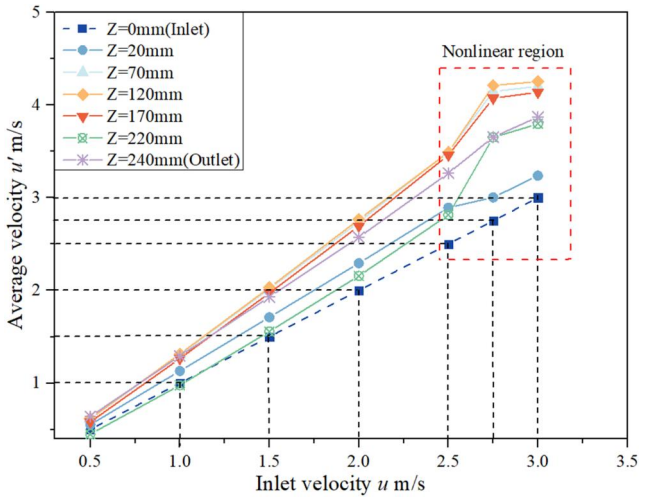

Figure 6. The influence of inlet gas velocity on the average air velocity of different cross-sections.

Figure 7(a) shows the pressure distribution of the centerline of the XOY section, and Figure 7(b) shows the pressure distribution contour of the section. In Figure 7(a), it can be observed that the pressure value decreases gradually with an increase in the Z value, and the pressure value first decreases and then increases gradually with an increase in the X value, which corresponds to Figure 5. The pressure distribution at different cross-sections in Figure 7(b) is uneven. The V-shaped cross region is the area where two

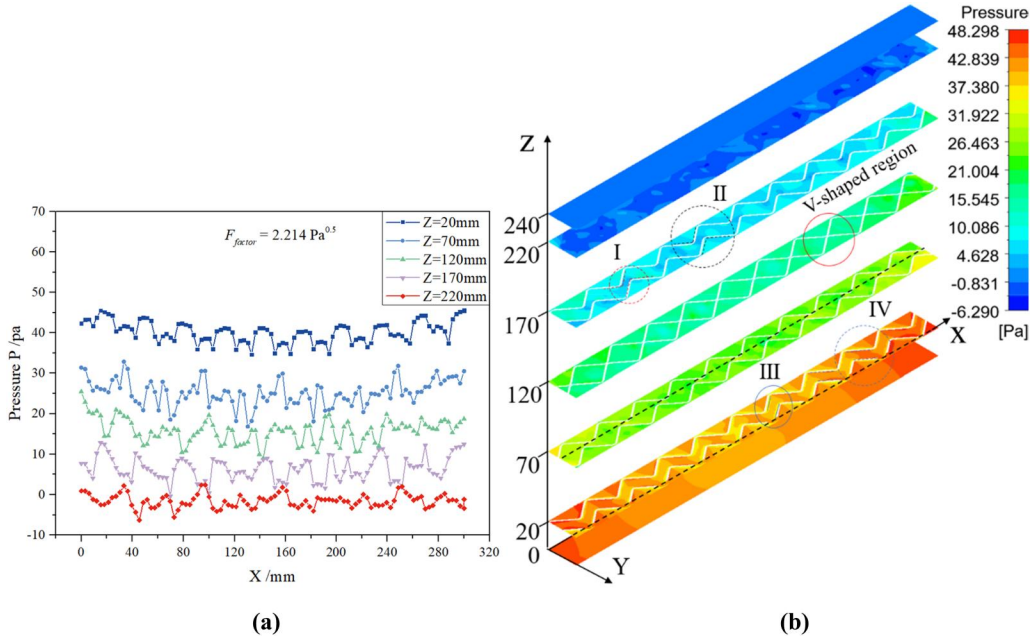

(a) **(b)**

Figure 7. Pressure distribution diagram of XOY section at different locations. (a) Section centreline pressure distribution. (b) Contour of cross-sectional pressure distribution.

adjacent corrugated plates are in close contact with each other. At the peak (Region I) above the V-shaped region ($Z = 70$ mm and $Z = 170$ mm), there is a higher pressure relative to the valley (Region II), which can be attributed to flow stagnation phenomena forming dead zones at the V-shaped intersections, and the upper peak valley shows lower pressure. At the center of the V-shaped region ($Z = 120$ mm), the pressure distribution is relatively uniform. At the cross-section below the V-shaped region (Z = 20 mm), the pressure on the impact surface (Region IV) of the airflow in the channel is relatively higher than that on the leeward surface (Region III), due to the influence of the rising airflow on the impact surface.

Pressure contour under different parameter conditions

CFD simulations enable a visual analysis of the internal flow field within the model. The structural characteristics of the corrugated plate and the specified simulation conditions play a significant role in shaping the internal pressure distribution. Therefore, we analyzed the pressure contour of the XOZ plane at the center of the corrugated plate under different parameters.

Figure 8(a)–(c) show the pressure distributions under different F_{factor}. Owing to the existence of the corrugated structure, the area where the pressure drop changes in the packing exhibits obvious stratification, and the pressure gradient line is arc-shaped (Figure 8a). An obvious V-shaped pressure distribution was observed at the junction of the corrugated plate. After the airflow passed through the V-shaped structure, the pressure decreased because the flow space at the V-shaped intersection of the corrugated plate was small and the resistance was large, which hindered the gas flow. With an increase in F_{factor}, the curvature of the circular arc pressure gradient line increases, and the range of the negative pressure zone gradually decreases. This is mainly due to the increase in the initial energy of the gas. The turbulence effect was enhanced when the gas passed through the corrugated plate, and the gas disturbance was large.

The opening configuration of corrugated plate significantly influences the packing porosity and the associated flow characteristics. According to the principles of porous media flow, an increase in the opening diameter of the corrugated plate enhances the overall packing porosity, which in turn provides additional bypass channels for airflow. The pressure distribution contours of the different corrugated plate holes showed in Figure 8(d)–(f). With an increase in the opening diameter of the corrugated plate, the high-pressure area at the center of the inlet area gradually increased, the negative-pressure area at the outlet area gradually decreased. Interestingly, the range of pressure variation remains relatively unaffected by the opening diameter. In Figure 9, we provide a detailed mechanistic analysis to elucidate the underlying mechanisms and relationships observed in the system.

Figure 8(g)–(i) show the pressure distributions at different corrugated plate inclination angles. In a packing veneer with a large corrugated inclination angle, the height of the diamond area formed by the corrugation is larger (black frame line in the figure), and the gas flux is larger. As shown in the figure, the corrugation angle decreased, the high-pressure area at the center of the inlet region gradually increased, the curvature of the arc-shaped pressure gradient line decreased, and the layering of different colors in the pressure distribution diagram was narrower and faster than that of the large corrugation inclination. This is closely related to the shape of the flow channel, which is composed of corrugations. This is because the local loss at the inlet decreases with an increase in the inclination angle, and the gas velocity in the gap inside the corrugated plate increases with an increase in the inclination angle. The resulting reduces gas turbulence results in a significant reduction in pressure loss owing to frictional resistance.

Figure 8(j)–(l) show the pressure distribution at different corrugated tooth angles. It can be observed from the figure that when the tooth angle is small, the number of cross-shaped areas inside the corrugated plate significantly increases (V-shaped junction area), and the curvature of the pressure gradient line is also larger. When the tooth angle was smaller, the pressure distribution was more uniform compared to the large tooth angles. The smaller the tooth angle, the greater the pressure difference, resulting in a higher pressure drop and stronger gas resistance

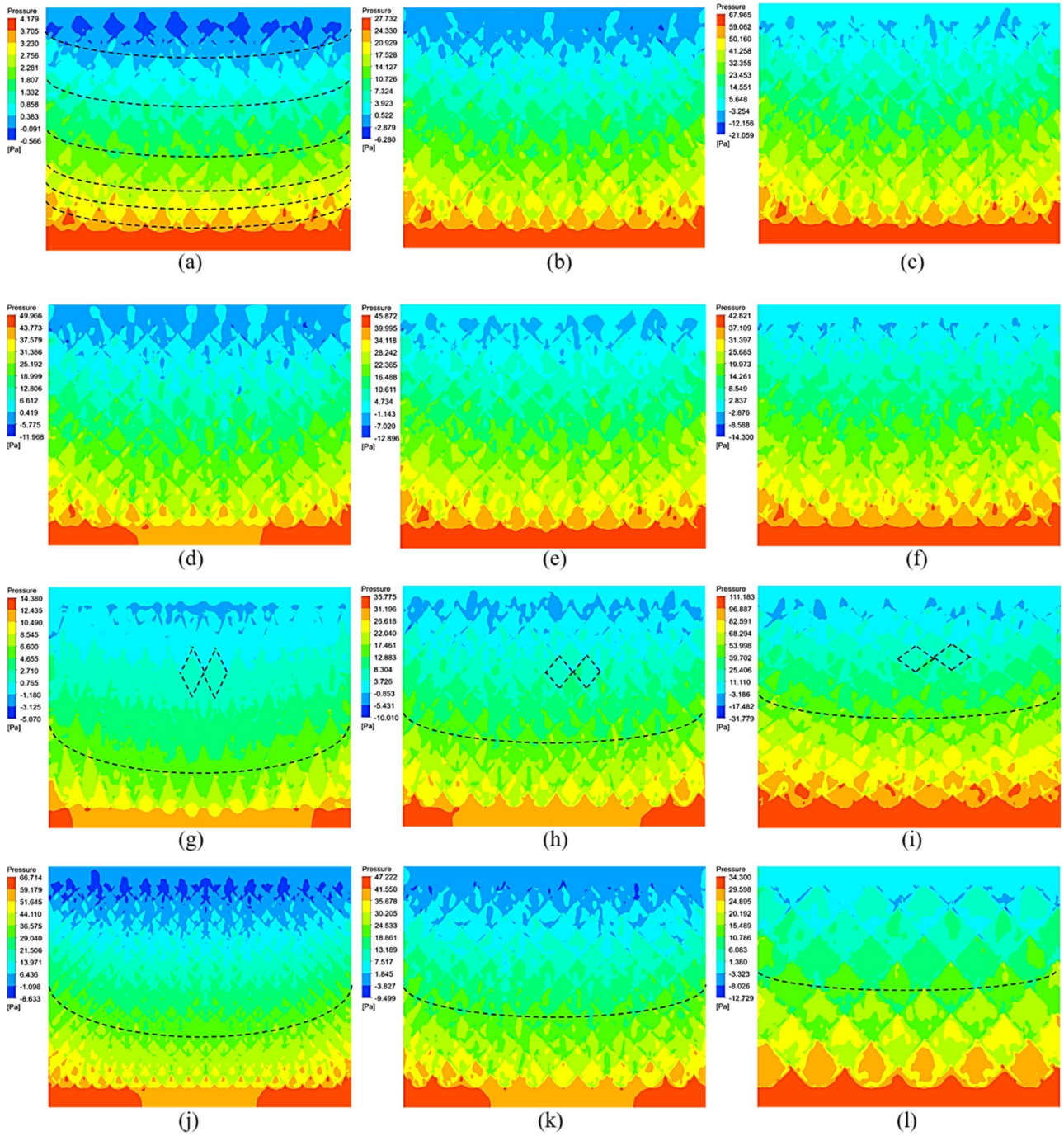

Figure 8. Pressure contours for different simulation parameters: (a) $F_1 = 0.553\,\mathrm{Pa}^{0.5}$, (b) $F_2 = 1.66\,\mathrm{Pa}^{0.5}$, (c) $F_3 = 2.767\,\mathrm{Pa}^{0.5}$ ($\delta = 1\,\mathrm{mm}$, $d = 6\,\mathrm{mm}$, $l = 12.5\,\mathrm{mm}$, $\theta = 45°$, $\beta = 90°$), (d) $d_1 = 4\,\mathrm{mm}$, (e) $d_2 = 6\,\mathrm{mm}$, (f) $d_3 = 8\,\mathrm{mm}$ ($F_{factor} = 2.214\,\mathrm{Pa}^{0.5}$, $\delta = 1\,\mathrm{mm}$, $l = 12.5\,\mathrm{mm}$, $\theta = 45°$, $\beta = 90°$), (g) $\theta_1 = 70°$, (h) $\theta_2 = 50°$, (i) $\theta_3 = 30°$ ($F_{factor} = 2.214\,\mathrm{Pa}^{0.5}$, $\delta = 1\,\mathrm{mm}$, $d = 6\,\mathrm{mm}$, $\beta = 90°$), (j) $\beta_1 = 40°$, (k) $\beta_1 = 80°$, (l) $\beta_1 = 120°$ ($F_{factor} = 2.214\,\mathrm{Pa}^{0.5}$, $\delta = 1\,\mathrm{mm}$, $d = 6\,\mathrm{mm}$, $\theta = 45°$).

effect. This is in direct contrast to the effect of the corrugation inclination angle.

Effect of inlet gas velocity on different cross-section pressure and gas velocity

To further investigate the flow characteristics inside the corrugated plate model, the average cross-sectional pressures and gas velocities under different F_{factor} were quantitatively studied. The cross-sectional positions are shown in Figure 7(b).

Figure 10 shows the relationship between the average pressure of the different sections and F_{factor}. When F_{factor} is the same, the average pressures of the inlet and packing regions decrease

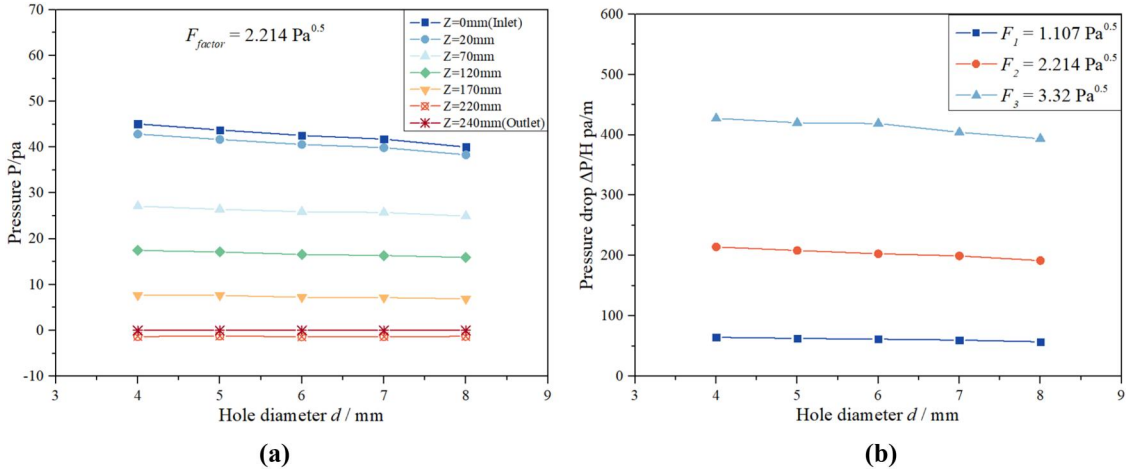

Figure 9. The influence of hole diameter on pressure distribution and pressure drop. (a) Pressure distribution. (b) Pressure drop.

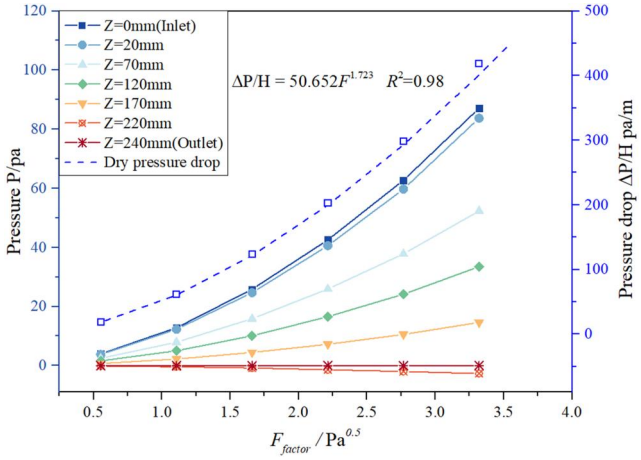

Figure 10. The influence of F_{factor} on the average pressure of different cross-sections.

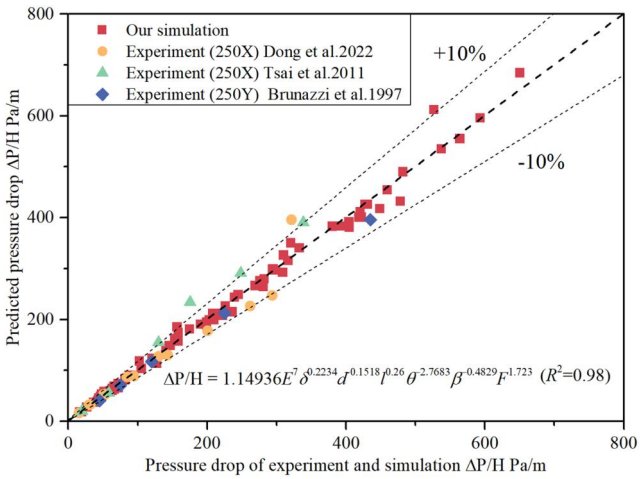

Figure 11. Deviation between simulated data and empirical data.

gradually with an increase in Z, which corresponds to the relevant description in Figure 5. However, it is interesting that the average pressure of the section showed an upward trend with an increase in the Z value in the outlet region (220 mm $< Z <$ 240 mm), and the center of the negative pressure area appeared at the end of the corrugated packing outlet. The variation in cross-sectional average pressures can be further explained by considering the flow dynamics. In the inlet and packing regions, the average pressures increase with higher F_{factor}. The higher F_{factor} correspond to increased flow rates, which in turn elevate the pressure requirements to overcome the system's resistance. In contrast, the outlet region exhibits a more complex response, with the average pressure remaining relatively constant or slightly decreasing as the F_{factor} increases. This discrepancy can be attributed to the changing flow patterns and momentum distribution within the outlet section, where the pressure recovery effects become more pronounced at higher flow rates. The corresponding pressure-drop relationship under this condition is shown in Figure 10. The pressure drop increases with F_{factor} increasing and exhibits a power-function distribution. We fitted a pressure drop curve based on the simulation data to predict the pressure drop change, as in Figure 11 of Equation (7). The structural parameters of corrugated plate were brought into Equation (7) respectively, the equation is shown in Figure 10.

Figure 6 illustrates the correlation between average gas velocity at various cross-sections and

inlet velocity. Below the critical threshold of 2.5 m/s, the cross-sectional velocity in the packing bed demonstrates linear proportionality to the inlet velocity. Beyond 2.5 m/s, the velocity profile transitions to nonlinear behavior accompanied by heterogeneous velocity distribution within the packed region. This regime shift is attributed to enhanced flow separation and intensified turbulent fluctuations resulting from elevated gas velocities. Computational modeling reveals that internal cross-sectional velocities consistently surpass the inlet velocity, with velocity maxima localized near the central axis of the packing bed. Notably, both the packing inlet ($Z = 20$ mm) and outlet ($Z = 220$ mm) exhibit velocities marginally exceeding the initial inlet velocity ($Z = 0$ mm). This phenomenon suggests the occurrence of localized flow acceleration and deceleration mechanisms during gas through the packings.

Effect of corrugated plate structural characteristics on pressure distribution and pressure drop

In this section, the CFD modeling is employed to systematically investigate the pressure distribution characteristics and pressure drop phenomena across corrugated plates with varying structural parameters (corrugation thickness, hole diameter, hole spacing, corrugation inclination angle, and tooth angle). This comprehensive analysis aims to elucidate the hydrodynamic performance of structured packings with different geometric configurations, thereby providing critical insights for optimizing mass transfer efficiency in industrial separation processes.

The influence of corrugation thickness on pressure distribution and pressure drop

Figure 12(a) shows the effect of different corrugated plate thicknesses on the cross-sectional pressure. As the thickness of corrugated plate increased, the cross-sectional pressures at different positions in the inlet and packing regions continued to increase. However, the trend of increasing cross-sectional pressure gradually becomes gentle with an increase in Z, whereas the pressure in the outlet region remains unchanged or decreases. The pressure drop is proportional to the thickness at different F_{factor} (Figure 12b). The larger the F_{factor}, the higher the slope of the pressure drop curve (corresponding to the imaginary line in the graph and the slope value k obtained by fitting) (Sebastia-Saez et al. 2015). However, the thickness of the corrugated plate decreases from 1.4 mm to 0.15 mm under different F_{factor}, and the pressure drop of packing is reduced by approximately 43.6%. Theoretically, the dry pressure drop of the packing primarily originates from three factors (Owens et al. 2013): local loss at the inlet, gas-to-gas friction between vertical crossflow channels, and turning losses at the transition layers and corrugation corners. As the corrugated plate thickness increases, the cross-sectional area of the packing inlet channel exhibits a significant reduction, leading to enhanced gas barrier performance. This geometric modification is accompanied by a

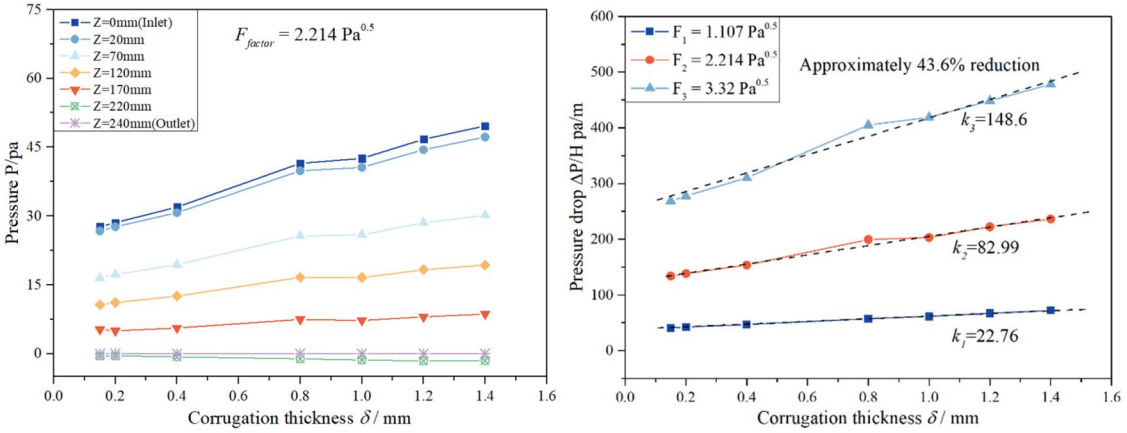

Figure 12. The influence of corrugated plate thickness on pressure distribution and pressure drop. (a) Pressure distribution. (b) Pressure drop.

concomitant decrease in both internal channel dimensions and material porosity within the packing structure. The resultant confinement effect amplifies gas-phase interactions through intensified intermolecular collisions and viscous friction phenomena. Consequently, these combined effects manifest as a substantial elevation in both pressure gradient and specific flow resistance across the packings (Sun et al. 2021a).

The influence of hole diameter on pressure distribution and pressure drop

Opening holes in corrugated plate packing is a means of improving the mass transfer efficiency of packing, which helps achieve a uniform distribution of gas-liquid phases. Different hole diameter can have a certain impact on the porosity of packings, thereby changing the pressure drop performance.

Figure 9(a) shows the relationship between the average pressure at different cross-sections and the diameter of corrugated plate opening. Corresponding to the pressure contour, the average pressure in the inlet and packing regions gradually decreased with an increase in the aperture, and the trend of the change was relatively gentle and linear. The variation in aperture had almost no effect on the average pressure in the outlet region. From the average pressure drop shown in Figure 9(b), the pressure drop decreased as the hole diameter increased. This is primarily because the small holes in the packing plate contribute to additional flow resistance by partially dissipating the kinetic energy of the airflow. During gas passage through the pore structures, turbulent mixing phenomena occur that enhances the collision between gases and generates additional local turbulence, thereby elevating both flow resistance coefficient and pressure drop (Isoz and Haidl 2018). However, increasing the hole diameter also increased the porosity, leading to a decrease in the resistance of the gas phase when passing through the packing layer and reducing the pressure drop loss. The interaction between the two competing mechanisms leads to the results shown in Figure 9(b). The opening of the corrugated plates increases the packing capacity, provides more channels for fluid infiltration and mixing, and has a beneficial effect on the mass transfer efficiency.

The influence of hole spacing on pressure distribution and pressure drop

In commercial packings, the hole spacing is one of the most variable parameters. Figure 13(a) shows the relationship between the average cross-sectional pressure and the spacing between the holes. The cross-sectional pressure gradually increased with the hole spacing. The inlet and packing area were more obvious. The increase in hole spacing actually results in a decrease in the porosity of the corrugated plates. Reduction in hole density lead to a decrease in airflow bypassing, resulting in a reduction of local turbulence, thereby decreasing the likelihood of gas collisions (Luo et al. 2008), and the influence of holes on the flow resistance decreased. Consequently, the main impediment to airflow becomes the

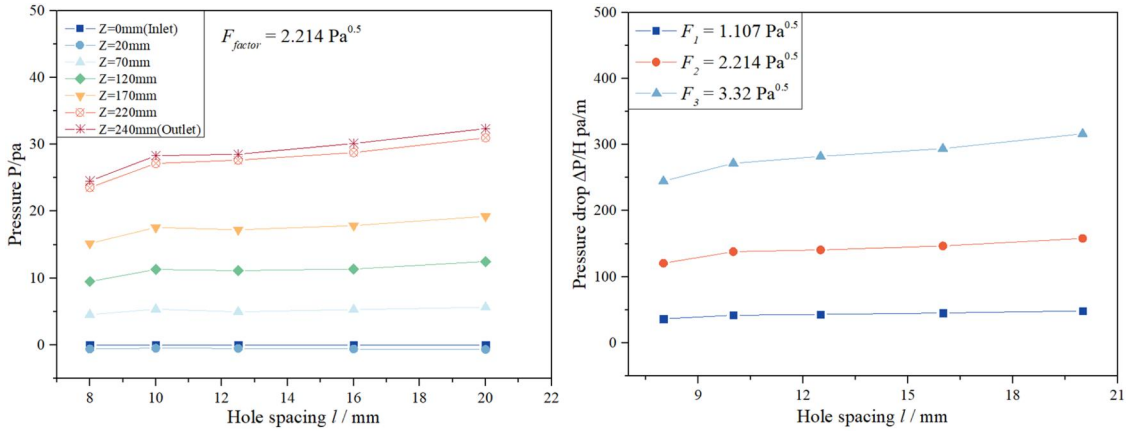

Figure 13. The influence of hole spacing on pressure distribution and pressure drop. (a) Pressure distribution. (b) Pressure drop.

corrugated plate, whose obstructive effect on the airflow is intensified, thereby increasing the pressure loss. The turbulence induced by the holes lead to energy dissipation within the system, although the impact may be relatively modest; however, the more favorable aspect of perforation is that it offers additional channels for fluid mixing, thereby enhancing the mass transfer capabilities. The variation pattern of the pressure drop with the hole spacing under different F_{factor} in Figure 13(b) is the same as that in Figure 13(a). And the larger the F_{factor}, the more significant the effect of hole spacing on pressure drop. The preceding discussion does not address the positional parameters of holes on corrugated plates, which may exert significant influences on hydrodynamic performance. These critical aspects will be systematically investigated in forthcoming research.

The influence of corrugated inclination angle on pressure distribution and pressure drop

The corrugated inclination angle has a profound impact on dry-wet pressure drop (Yu et al. 2018). The corrugated inclination angle is defined as the angle between the corrugation channel and radial of the column, which mainly guides the gas flow. Figure 14(a) shows the relationship between the average pressure and corrugated inclination angle at different cross-sections. As the corrugation angle increased, the average pressure at the inlet and packing cross-sections gradually decreased in the power function relationship, whereas the outlet region remained unchanged or increased. The figure shows that the average pressure change in different sections was more evident when the corrugated inclination angle was less than 50°, and the pressure change was smoother when the corrugated inclination angle was greater than 50°. This is because the corrugated inclination angle, which is more inclined toward the overall gas flow direction, is larger, and the gas resistance is smaller.

Figure 14(b) shows the pressure drop of corrugated plate decreases with an increase in the corrugated inclination angle, exhibiting a power function. The larger the corrugated inclination angle, the greater is the gas flux. The geometric modification of flow channels exerts more pronounced effects on pressure dissipation when the gas tends to flow along the corrugation direction. When the overall flow direction of the gas tended to be consistent, the change in the flow channel angle had a greater influence on the pressure drop loss. This is because the gap velocity increases as the inclination angle decreases, leading to an increasing gas turbulence which results in a significant increase in pressure loss owing to friction resistance. Based on the pressure drop in the corrugation, the simulation results were subjected to multiple linear regression and Equation (7) in Figure 11 is obtained. The fitted curve obtained through parametric substitution in the derived equation (shown in Figure 14) exhibit excellent agreement with numerical results. In terms of its index, the inclination angle parameter exerts stronger influence than the F_{factor}. When the corrugated angle is below 50°, the pressure drop increases sharply as the angle decreases, which

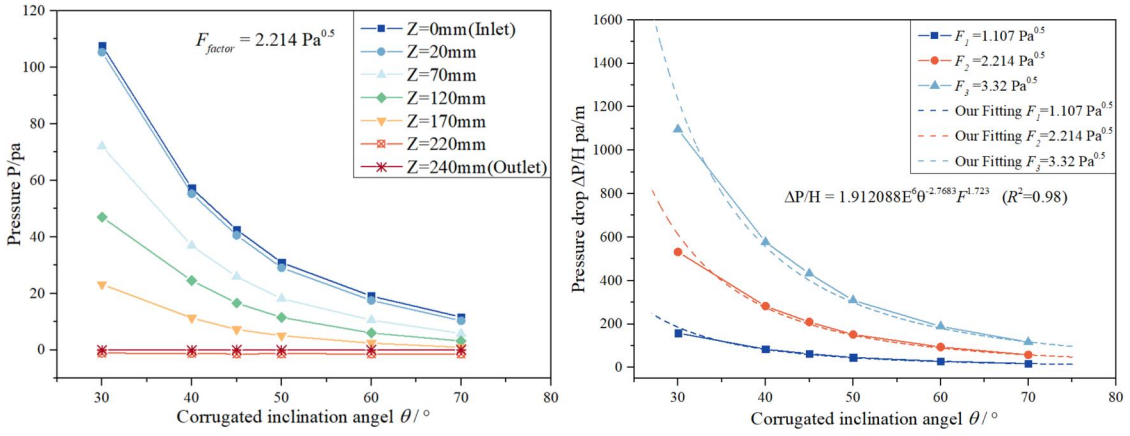

Figure 14. The influence of corrugated inclination angle on pressure distribution and pressure drop. (a) Pressure distribution. (b) Pressure drop.

aligns with the outcomes reported by Olujić et al. (2000). However, when the pressure drop is greater than 50°, the pressure drop decreases more slowly as the angle increases, suggesting possible saturation of flow obstruction effects induced by corrugation angle variations.

The influence of corrugated tooth angle on pressure distribution and pressure drop

The tooth angle of the corrugated packing is a key factor affecting the shape and size of the gas-liquid flow channels. Figure 15(a) shows the relationship between the pressure of various cross sections and corrugated tooth angle. For models with different corrugated tooth angles, we can construct the model by keeping the corrugation height the same and adjusting the length of the corrugated hypotenuse and the wavelength. Only the influence of corrugated tooth angle on pressure was explored here, without considering the effect of specific surface area. The pressure across various cross-sections increases with the decrease of tooth angle, which has a significant effect on the pressure in the inlet and packing regions and the effect of tooth angle on pressure is more pronounced when the tooth angle is less than 60°. This is mainly owing to the presence of a certain thickness of the corrugated plate used in the simulation. When the tooth angle decreases, the flow channels inside the packing become narrower, resulting in increased local frictional resistance losses (manifested at the inlet and inside of the packing). At the same time, the V-shaped area inside the corrugated plate significantly increases, which is equivalent to increasing the tortuosity of the channel (Figure 7), and the collision of gases at the intersection enhances turbulent dissipation. This geometric modification amplifies fluid resistance through two principal mechanisms: first, enhanced collision frequency between gas streams at intersecting channels, and second, intensified frictional dissipation at these junctions. According to the principles of fluid mechanics, an increase in flow resistance will inevitably lead to an increase in pressure drop when the fluid passes through the packing layer.

Figure 15(b) shows the relationship between the corrugated tooth angle and pressure drop under different F_{factor}, which decreases with an increase in the corrugated tooth angle. This is similar to the effect of the wavelength of a structural sinusoidal corrugated plate on the pressure drop reported by Wang et al. (2022). When the tooth angle was less than 60°, the pressure drop decreased significantly, particularly under a high F_{factor}, and the pressure drop changes at other tooth angles were gentler. As the corrugated tooth angle increased, the space of the gas channel increased, the void ratio increased simultaneously, and the inlet loss decreased; therefore, the pressure drop decreased.

Summary and outlook on structural optimization

Based on the above study regarding the impact of structural parameters of the corrugated plate on

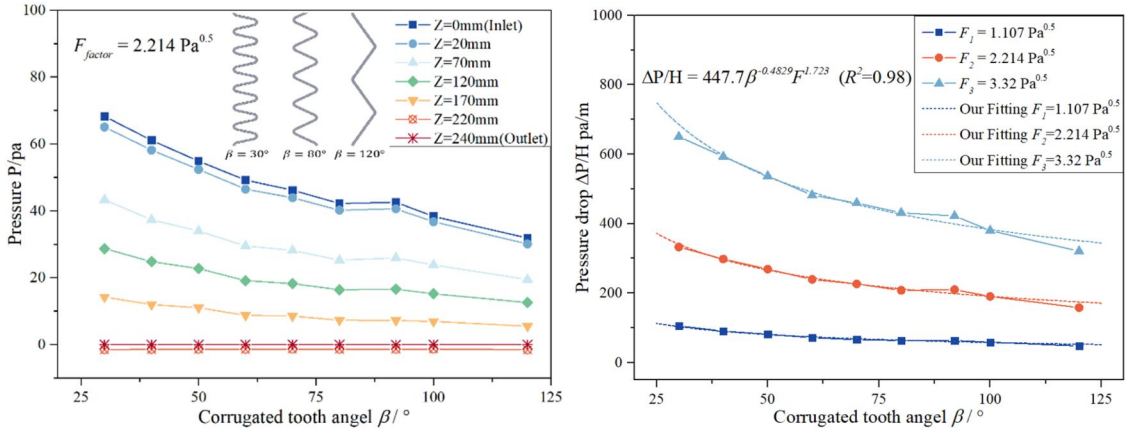

Figure 15. The influence of corrugated tooth angle on pressure distribution and pressure drop. (a) Pressure distribution. (b) Pressure drop.

pressure drop, the effects of the corrugated plate thickness, hole diameter, hole spacing corrugation inclination, and tooth angle on the pressure drop exhibit a linear relationship. Therefore, multiple linear fitting was performed by considering various factors, and Equation (7) was obtained to predict the pressure drop changes under different structural parameters. In the small inset at the top left of Figure 4(b), the structural conditions of the corrugated plates from Brunazzi et al. and Sun et al. are input into Equation (7), yielding the dashed lines shown in the figure (Brunazzi and Paglianti 1997; Sun et al. 2021a). The average errors of the pressure drop data were 9.2% and 6.5%. In the parity plot depicted in Figure 11, we present a comparison and validation of the pressure drop prediction equation against the experimental data from Tsai et al. Dong et al. for the 250X packing, along with our simulation data (Dong et al. 2022; Tsai et al. 2011). The predicted pressure drop values demonstrated excellent agreement with the experimental data, with the majority of predictions falling within 10% of the measured values, indicating the robust reliability of the model.

$$\frac{\Delta P}{H} = 1.14936E^{7}\delta^{0.2234}d^{-0.1518}l^{0.26}\theta^{-2.7683}\beta^{-0.4829}F^{1.723}R^{2} = 0.98 \tag{7}$$

As a critical indicator for evaluating the operational efficiency and energy consumption of packed towers, pressure drop optimization plays a significant role in system design. This study was based on the conventional Mellapak 250Y packing and focused on investigating the influence of its structural parameters on the pressure drop performance of packing. From the perspective of pressure drop, ideal packing should have the following characteristics: a thinner plate thickness, a larger hole diameter, a hole spacing of approximately 10 mm, a corrugation angle ranging from 45° to 60°, and a corrugation tooth angle between 80° and 100°.

According to Equation (7), the corrugation inclination angle exerts a pronounced effect on pressure drop. An increase in the corrugation inclination angle significantly reduces the pressure drop; however, it also has adverse effects, such as high gas flow rates, low liquid holdup, and short contact time. Future research will focus on the structural optimization of packing at a larger corrugation inclination angle to improve mass transfer efficiency.

Conclusions

The hydrodynamic performance of high-fidelity corrugated plate packing under various structural parameters was numerically investigated using the k-ω SST model. By analyzing the flow field distribution and pressure drop characteristics, the underlying mechanisms through which different structural parameters influence the packing's hydrodynamic behavior were systematically elucidated. An innovative method for predicting dry pressure drop under different structural parameters was proposed. The conclusions are as follows:

Nonuniform pressure distribution was observed within the packing structure, characterized by distinct pressure gradients with relatively high pressure near the wall surfaces and low pressure in the central region. The pressure gradient contour displayed an arcuate configuration. There was a V-shaped cross distribution at the junction of the corrugated plate, exerting substantial impact on pressure dissipation. The most noticeable pressure drop occurred in the initial segment of packing region. As the F_{factor} increased, the pressure in the inlet and packing region intensified, while the pressure in the outlet region had less effect. The internal velocity of the packing surpassed the inlet gas velocity, accompanied by localized flow acceleration/deceleration phenomena.

The relationship between dry pressure drop and the structural parameters of the corrugated plate can be expressed as: $\Delta P/H = 1.14936E^{7}\delta^{0.2234}d^{-0.1518}l^{0.26}\theta^{-2.7683}\beta^{-0.4829}F^{1.723}$. An increase in corrugated plate thickness led to a linear pressure increases in both inlet and packing regions. Changing the aperture had no significant effect on pressure drop. Highly perforated packings had lower dry pressure loss than the low perforated ones. The dry pressure drop of packing decreased with an increase in the corrugated inclination angle and corrugated tooth angle, but increased along with the F_{factor}. The dry pressure drop of corrugated plate packing was synergistically

influenced by the hydrodynamic behavior and energy dissipation regulated by structural parameters. The plate thickness, inclination angle, and tooth angle could change the cross-sectional area of fluid channels and the tortuosity of flow paths. The hole diameter and spacing would affect the flow channel and the intensity of turbulent disturbance. The pressure drop depended on the synergistic effect among structural parameters, and comprehensive optimization was required to balance the pressure drop and mass transfer efficiency.

The results of this study are crucial for understanding the hydrodynamic performance of structured packings. These insights provide a foundation for further optimizing the design of structured packing.

Authors' contribution

All authors contributed to the study conception and design. The first draft of the manuscript was written by Enhua Zheng, Lina Tang, Zhixiang Xia, Mengxiang Fang, and all authors commented on previous versions of the manuscript. All authors read and approved the final manuscript.

Disclosure statement

The authors report there are no competing interests to declare.

Funding

This work is supported by National Key R&D Program of China (2023YFE0199300) and "the Fundamental Research Funds for the Central Universities" (2022ZFJH004).

ORCID

Enhua Zheng http://orcid.org/0000-0002-1197-7314

Data availability statement

The data that support the findings of this study are available on request from the corresponding author. The data are not publicly available due to privacy or ethical restrictions.

References

Al-Maqaleh YN, Raimondi DM, Fletcher DF, Rouzineau D, Meyer M. 2022. Experimental and numerical investigation of dry pressure drop of 3D-printed structured packings for gas/liquid contactors. Chem Eng Process. 175:108912. doi: 10.1016/j.cep.2022.108912.

Ambekar AS, Peters EAJF, Hinrichsen O, Buwa VV, Kuipers JAM. 2024. Understanding the role of perforations on the local hydrodynamics of gas-liquid flows through structured packings. Chem Eng J. 486:150084. doi: 10.1016/j.cej.2024.150084.

Amini Y, Karimi-Sabet J, Esfahany MN. 2016. Experimental and numerical simulation of dry pressure drop in high-capacity structured packings. Chem Eng Technol. 39(6): 1161–1170. doi: 10.1002/ceat.201500477.

Billet R. 1987. Performance of low pressure drop packings. Chem Eng Commun. 54(1–6):93–118. doi: 10.1080/00986448708911901.

Brunazzi E, Paglianti A. 1997. Mechanistic pressure drop model for columns containing. AIChE J. 43(2):317–327. doi: 10.1002/aic.690430205.

Dong WF, Fang MX, Liu ZJ, Han T, Gao L, Wang T, Wang QH. 2022. Study on chemical absorption absorber with polypropylene packing for Guohua Jinjie CCS demonstration project. Int J Greenhouse Gas Control. 114:103581. doi: 10.1016/j.ijggc.2022.103581.

Fair JR, Seibert AF, Behrens M, Saraber PP, Olujic Z. 2000. Structured packing performance experimental evaluation of two predictive models. Ind Eng Chem Res. 39(6): 1788–1796. doi: 10.1021/ie990910t.

Haghshenas Fard M, Zivdar M, Rahimi R, Nasr Esfahani M, Afacan A, Nandakumar K, Chuang K T. 2007. CFD simulation of mass transfer efficiency and pressure drop in a structured packed distillation column. Chem Eng Technol. 30(7):854–861. doi: 10.1002/ceat.200700011.

Haroun Y, Raynal L. 2016. Use of computational fluid dynamics for absorption packed column design. Oil Gas Sci Technol Rev IFP Energies Nouvelles. 71(3):43. doi: 10.2516/ogst/2015027.

Hosseini SH, Shojaee S, Ahmadi G, Zivdar M. 2012. Computational fluid dynamics studies of dry and wet pressure drops in structured packings. J Ind Eng Chem. 18(4):1465–1473. doi: 10.1016/j.jiec.2012.02.012.

Isoz M, Haidl J. 2018. Computational-fluid-dynamics analysis of gas flow through corrugated-sheet-structured packing: effects of packing geometry. Ind Eng Chem Res. 57(34):11785–11796. doi: 10.1021/acs.iecr.8b00676.

Larachi FC, Petre CF, Iliuta I, Grandjean B. 2003. Tailoring the pressure drop of structured packings through CFD simulations. Chem Eng Process. 42(7):535–541. doi: 10.1016/S0255-2701(02)00073-9.

Liu QZ, Zou ZY, Xiong XH, Li SS, Li CD, Wang Z, Wang GC, Zhang XB, Li GB, Zhang ZW. 2024. Numerical simulation of hydrodynamic properties of perforated corrugated sheet materials. Mater Today Commun. 41: 110956. doi: 10.1016/j.mtcomm.2024.110956.

Luo SJ, Fei WY, Song XY, Li HZ. 2008. Effect of channel opening angle on the performance of structured packings. Chem Eng J. 144(2):227–234. doi: 10.1016/j.cej.2008.01.026.

Macfarlan LH, Seibert AF, Phan MT, Eldridge RB. 2021. CFD-based study on structured packing geometry. Chem Eng Sci. 243:116767. doi: 10.1016/j.ces.2021.116767.

Macfarlan LH, Phan MT, Eldridge RB. 2022. Structured packing geometry study for liquid-phase mass transfer and hydrodynamic performance using CFD. Chem Eng Sci. 249:117353. doi: 10.1016/j.ces.2021.117353.

Olenberg A, Kenig EY. 2020. Numerical investigation of liquid flow morphology in structured packings. Chem Eng Sci. 219:115559. doi: 10.1016/j.ces.2020.115559.

Olujić Ž, Seibert AF, Fair JR. 2000. Influence of corrugation geometry on the performance of structured packings: an experimental study. Chem Eng Process. 39(4):335–342. doi: 10.1016/S0255-2701(99)00095-1.

Olujic Z, Jansen H, Kaibel B, Rietfort T, Zich E. 2001. Stretching the capacity of structured packings. Ind Eng Chem Res. 40(26):6172–6180. doi: 10.1021/ie010323j.

Olujić Z, Rietfort T, Jansen H, Zich E. 2015. Performance characteristics of an intermediate area high performance structured packing. Chem Eng Res Des. 99:14–19. doi: 10.1016/j.cherd.2015.03.004.

Owens SA, Perkins MR, Eldridge RB, Schulz KW, Ketcham RA. 2013. Computational fluid dynamics simulation of structured packing. Ind Eng Chem Res. 52(5):2032–2045. doi: 10.1021/ie3016889.

Petre CF, Larachi F, Iliuta I, Grandjean BPA. 2003. Pressure drop through structured packings: break-down into the contributing mechanisms by CFD modeling. Chem Eng Sci. 58(1):163–177. doi: 10.1016/S0009-2509(02)00473-6.

Raynal L, Royon-Lebeaud A. 2007. A multi-scale approach for CFD calculations of gas-liquid flow within large size column equipped with structured packing. Chem Eng Sci. 62(24):7196–7204. doi: 10.1016/j.ces.2007.08.010.

Roselló Segado A, Carrillo De La Fuente FM, Aguilar A. 2002. Laboratory data of structured gauze packings as a base for scale-up in distillation. Chem Eng Commun. 189(11):1470–1484. doi: 10.1080/00986440214995.

Said W, Nemer M, Clodic D. 2011. Modeling of dry pressure drop for fully developed gas flow in structured packing using CFD simulations. Chem Eng Sci. 66(10):2107–2117. doi: 10.1016/j.ces.2011.02.011.

Sebastia-Saez D, Gu S, Ranganathan P, Papadikis K. 2015. Micro-scale CFD modeling of reactive mass transfer in falling liquid films within structured packing materials. Int J Greenhouse Gas Control. 33:40–50. doi: 10.1016/j.ijggc.2014.11.019.

Singh RK, Galvin JE, Sun X. 2017. Hydrodynamics of the rivulet flow over corrugated sheet used in structured packings. Int J Greenhouse Gas Control. 64:87–98. doi: 10.1016/j.ijggc.2017.07.005.

Sun B, Bhatelia T, Utikar RP, Evans GM, Pareek VK. 2021a. Study on hydrodynamic performance of structured packings for gas-liquid flow: effects of geometry parameters. Chem Eng Res Des. 167:318–326. doi: 10.1016/j.cherd.2021.01.003.

Sun B, Bhatelia T, Utikar RP, Evans GM, Pareek VK. 2021b. Hydrodynamics of a novel 3D printed structured packing – SpiroPak. Chem Eng Process. 167:108533. doi: 10.1016/j.cep.2021.108533.

Tsai RE, Seibert AF, Eldridge RB, Rochelle GT. 2011. A dimensionless model for predicting the mass-transfer area of structured packing. AIChE J. 57(5):1173–1184. doi: 10.1002/aic.12345.

Wang GC, Cai WF, Xie L, Zhang XB, Wang Y. 2022. CFD modeling and simulation of the hydrodynamics characteristics of packed column with structured sinusoidal corrugated sheets packings. Chem Eng Res Des. 183:56–66. doi: 10.1016/j.cherd.2022.04.038.

Yang L, Zhang L, Hu J, Li Y, Fang J, Yu Z, Xu W, Dong K, Qian W, Zhang H. 2024. Experiment and numerical study on thermal performance of counterflow wet cooling tower filled with double S-wave packing. Int J Therm Sci. 200:108984. doi: 10.1016/j.ijthermalsci.2024.108984.

Yu D, Cao D, Li Z, Li Q. 2018. Experimental and CFD studies on the effects of surface texture on liquid thickness, wetted area and mass transfer in wave-like structured packings. Chem Eng Res Des. 129:170–181. doi: 10.1016/j.cherd.2017.10.035.

Zakeri A, Einbu A, Svendsen F. 2012. Experimental investigation of pressure drop in structured packings. Chem Eng Sci. 73:285–298. doi: 10.1016/j.ces.2012.01.025.

Zhi XQ, Hu SY, Gu CJ, Qi YH, Qiu LM. 2023. Influence of structured packing geometric parameters on flow and mass transfer performance of liquid nitrogen and oxygen for cryogenic distillation. Cryogenics. 130:103647. doi: 10.1016/j.cryogenics.2023.103647.